Methodology to Stochastically Generate Synthetic 1-Minute Irradiance Time-Series Derived from Mean Hourly Weather Observational Data

Jamie M. Bright[1] , Peter G. Taylor[1,2,3] and Rolf Crook[1]

[1] Energy Research Institute, School of Chemical and Process Engineering, University of Leeds, Leeds (UK), LS2 9JT

[2] Sustainability Research Institute, University of Leeds, Leeds (UK)

[3] Centre for Integrated Energy Research, University of Leeds, Leeds (UK)

Abstract

Well geographically distributed high temporal resolution solar irradiance data is scarce, resulting in many studies using mean hourly irradiance time-series as an input. This research demonstrates that by taking readily available mean hourly meteorological observations of okta, wind speed, cloud height and atmospheric pressure; 1-minute resolution irradiance time-series that vary on a spatial dimension can be produced. The synthetic time-series temporally validates against observed 1-minute UK irradiance data with 99% K-S test confidence levels across 3 metrics of variability indices, ramp-rate occurrences and irradiance frequency. A new methodology is applied to existing research that produces two-dimensional cloud cover using a vector approach to add spatial correlation to irradiance time-series, as well as improvements to the clear-sky index calculations. The methodology is applied to a hypothetical configuration to demonstrate its capabilities.

Keywords: *irradiance generation, minute resolution, resource modelling, cloud edge enhancement.*

1. Introduction

Solar irradiance fluctuates on a 1-minute time scale or less (Sayeef et al., 2012) and is driven by the transport of atmospheric pollutants (Vindel and Polo, 2014), atmospheric losses, and cloud dynamics (Calinoiu, 2014). Large irradiance fluctuations can cause ramps in solar energy power generation outputs (Hummon et al., 2012), these power fluctuations can result in electrical problems and supply/demand issues such as over voltages in PV laden distribution grids (Widén et al., 2011). Furthermore, irradiance is dependent on geography, irradiance at locations across 1 km are affected by different optical losses as they can be obscured at different times. It is important, therefore, to utilise a solar irradiance data input that can capture these problematic fluctuations and spatial variations when theoretically considering power reliability and impacts on a high frequency time scale. Averaging solar irradiance data over different temporal frequencies results in loss of detail of the irradiance fluctuations. Figure 1 demonstrates how averaging irradiance data across different time-scales significantly underemphasises the actual incident irradiance fluctuations, as well as underestimating peak irradiance values.

Calibrated 1-min irradiance datasets are usually the output of isolated research projects and are often limited in duration, consistent measurement techniques, and geographic distribution. Sources of 1-min resolution irradiance data exist such as the World Radiation Monitoring Centre's Baseline Surface Radiation Network (BSRN), which will be used in a validation, however it is lacking in coarse geographical distribution. 1-hour resolution weather data, however, is widely collected and made available through national meteorological offices. This hourly data fails to capture the intermittent nature of solar irradiance (Sayeef et al., 2012); some solar irradiance models, therefore, use hourly datasets to artificially generate minutely irradiance time-series. Examples of such have been reviewed previously (Gueymard, 2012), with more notable methodologies using utilising a sun obscured type approach (Morf, 1998, 2011, 2013) and (Ehnberg and Bollen, 2005).

This paper presents a novel methodology that takes readily available mean hourly meteorological observation data of okta, wind speed, cloud height and atmospheric pressure; 1-minute resolution irradiance time-series that vary on a spatial dimension can be produced, which validate temporally against observed 1-minute UK irradiance data.

Selection and/or peer review under responsibility of Scientific Committee
doi:10.18086/swc.2015.07.02 Available at http://proceedings.ises.org

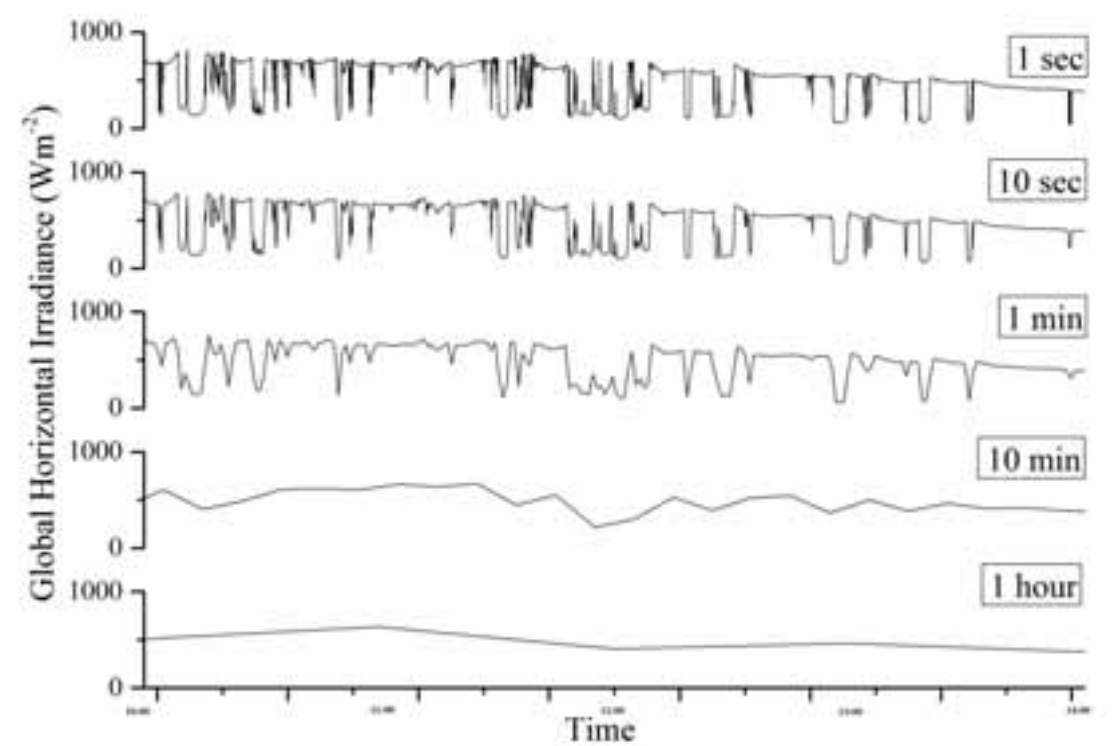

Fig. 1: Global horizontal incident irradiance in Leeds, UK on 25/06/2015 between the hours of 10:00 and 14:00. The data was logged using a horizontally-mounted silicon photodiode (BPW20) in short-circuit current mode with a linear current response converted to voltage with a transconductance amplifier, logged at 10 Hz using a 10-bit DAC. The data has been averaged across the timescales of, from top to bottom: 1 second, 10 seconds, 1 minute, 10 minutes and 1 hour.

2. Methodology

This work is an extension of the methodology by Bright et al. (2015) that demonstrated the success of taking mean hourly weather observation data to generate 1-min temporal resolution irradiance time-series. The original methodology has six distinct sections: cloud cover samples production, where descriptions of an hour of cloud are made; Markov chain production, produced through analysis of 12 years of mean hourly weather observation data to capture the patterns of transitions of each variable; the stochastic selection of variables, using probabilistic application of the variables guided by the Markov chains; calculation of global clear-sky irradiance, using standard irradiance modelling considering geography to determine the background irradiance; calculation of clear-sky index for each location, using statistics of optical losses derived as a function of the okta value; and finally calculation of incident irradiance upon an arbitrary plane, using methodologies from literature. For greater detail, the reader is referred to the work by Bright et al., (2015).

Significant developments have been made to the cloud cover samples production section and the calculation of clear-sky indices sections that allow for a spatial element to the previous temporal-only methodology. This section will discuss the production of cloud cover samples and their application in producing spatially correlating sun obscured time-series, and the updates to calculating the clear-sky indices and subsequent irradiance.

2.1 Cloud Cover Sample Production

Cloud cover samples are a description of an hour's cloud cover. The methodology is a sun-obscured type, which means that during periods when the sun is obscured, as indicated by the cloud cover sample, a clear-sky index value is applied to the global clear-sky irradiance. The clear-sky index is a fractional representation of the incident global horizontal irradiance from the available clear sky irradiance. Previously, the cloud cover samples were represented by a binary, single dimension vector describing each minute that

an arbitrary plane as obscured or unobscured, signified using 1s and 0s respectively. A new methodology is proposed that considers an area of sky with a randomly set number of clouds within it, as this will be moving across a static cluster with points of interest i.e. residential PV installations within a low voltage grid, each sample of cloud cover must represent the entire hour defined by the stochastic selection of the weather variables: cloud speed, u, and okta. The size of the area of sky is therefore a function of distance and time, 1.5km-by-u*3600, where 3600 is the number of seconds in an hour.

The cloud cover samples are lists of x and y coordinates for the centres of each cloud, and also includes their radii. The clouds are assumed to be circular with radii size adhering to the horizontal cloud length single power-law distribution (Wood and Field, 2011). The clouds' associated clear-sky indices are represented as optical thicknesses applied to all areas across the circle using a distribution that ranges from typical clear-sky indices lows of ~0.1, to highs of ~1.1, the implication of this is that across the circular cloud there will be sections above a clear-sky index of 1, indicating wispy or insignificant levels of cloud, whilst other areas indicate thicker sections, and therefore the clouds are not actually circular in application, instead the circle defines an area which cloud is allowed to form. In order to produce multiple samples, random numbers of clouds are selected, which are then given random x-y coordinates and radii drawn by the aforementioned distribution. The cloud cover fraction of each sample is analysed to determine the okta value, and is then sorted and stored appropriately in a larger matrix. Samples are then selected using an indexing based on the conditions stochastically selected through a Markovian process within the model simulation.

2.2 Clear-sky Fluctuations

Clear-sky indices fluctuate across different timescales. The cumulative probability distributions functions (CDF) for the frequency of occurrence of absolute step size changes for different time scales are shown in Lave et al. (2012). It is shown that 1-min and 1-hour data have very different statistics. To capture these fluctuations, the CDF profiles for the different time scales are applied to the clear-sky indices. Two vectors of fluctuations following the CDF profiles are drawn, one for clear periods, $\boldsymbol{F_0}$, the other for obscured periods, $\boldsymbol{F_1}$. For moments of obscured sky, the step changes are equally step downs as well as step ups.

To create $\boldsymbol{F_0}$ and $\boldsymbol{F_1}$, a step size change is selected following the appropriate cumulative distribution function, this increase is then linearly applied across the hour/10-min/minute, before being smoothed using a spline technique (using inbuilt Matlab functions (Matlab, 2012)) and can be represented for both as

$$\mathbf{F}_{(\mathbf{0}or\mathbf{1})}(t_0 : t_1) = \left(\mathbf{F}_{(\mathbf{0}or\mathbf{1}),t0} : T : 1 \pm s\right) \qquad \text{(eq. 1)}$$

$$s = \frac{\sum CDF_T < r}{100} \qquad \text{(eq. 2)}$$

where t_0 and t_1 are index references in minutes of current and future location within $\boldsymbol{F_{0or1}}$, T refers to the number of minutes within the operating frequency (when performing fluctuations on a 1-h period, T=60), $\boldsymbol{F_{t0}}$ refers to the fluctuation value at the previous index. The use of the colon, **:**, in the format $(t_0 : t_1)$ refers to the space within $\boldsymbol{F}$ between t_0 and t_1, and in the format $(x : n : y)$ refers to a linearly spaced vector starting at x and ending at y with n number of intervals. CDF_T refers to the appropriate cumulative probability distribution function, r is a random variate evenly distributed between 0 and 1, and finally s is the step size magnitude randomly extracted from the CDF.

2.3 Cloud Movement and Clear-sky Indices

Once the cloud cover samples are selected for each hour of the simulation, the samples are simulated to pass across the stationary targets within the spatial domain. To simulate the cloud direction, the locations are rotated in accordance with the cloud direction using rotational matrices as demonstrated in equation 3

$$\begin{bmatrix} x' \\ y' \end{bmatrix} = \begin{bmatrix} \cos\vartheta & -\sin\vartheta \\ \sin\vartheta & \cos\vartheta \end{bmatrix} \begin{bmatrix} x \\ y \end{bmatrix} \qquad \text{(eq. 3)}$$

where x and y denote the coordinates of the initial locations within the spatial domain, and x' and y' are the rotated coordinates by angle ϑ. The angle by which to rotate is determined using a normally distributed random walk, with standard deviation equal to 10, around a mean set to the previous cloud direction, this allows for gradual changes in direction. The cloud speed is determined stochastically (Bright et al., 2015) and so the cloud movements in relation to the locations of interest within the spatial domain are known.

The simulation works iteratively, progressing by one time-step at a time. Whilst the calculations are in a vectorised format, it is simplest to imagine a static rectangle with the locations of interest marked, being overlapped by a rectangle containing the clouds; at each moment it is determined whether or not a location is obscured by the cloud. For each iteration, the distance from the location of interest to the centre of each cloud within the sample is calculated. Firstly, let the length of the spatial domain be X_l and the length of the cloud sample be X_c, the coordinates of the location of interest and each cloud are (x_l',y_l') and (x_c,y_c) respectively. The distance from the location to the edge of the domain is

$$\partial x_l = X_l - x_l' \qquad \text{(eq. 4)}$$

while the distance from the cloud to the edge of the cloud environment is given by x_c. The overlap of domains is defined as the number of iterations, i, multiplied by the temporal resolution that the simulation is operating at, t. Therefore the distance in the x-direction from the location to the cloud, dx, is given by

$$\partial x = \partial x_l + x_c - it \qquad \text{(eq. 5)}$$

the distance along the y-axis from the location to the cloud is given by

$$\partial y = y_c - y_l' \qquad \text{(eq. 6)}$$

the horizontal distance from the location to the centre of the cloud is therefore calculated using Pythagoras' theorem as

$$d = \sqrt{\partial x^2 + \partial y^2} \qquad \text{(eq. 7)}$$

To produce a clear-sky indices vector for each location, the simulation enters an loop which cycles through each time step for the desired duration, and for each location. At each loop the locations are rotated according to the cloud movement direction as shown in equation 3, the x-y coordinates of each cloud sample are updated according to the cloud movement speed and time step before working through equations 4-7. At each loop it is determined if the location is covered by cloud. To do so, a logical *if* statement is applied, querying d against the radius of the cloud, r, such that

$$r > d \rightarrow B = 1 \text{ else } B = 0 \qquad \text{(eq. 8)}$$

where B is a Boolean matrix indicating the presence of cloud, and $\rightarrow$ denotes the use of a logical *if* statement. The iteration moves on until the end of the cloud sample. If a location moves beyond the sample

as it passes, the next sample is loaded and queried against using the same methodology.

B is used as a binary indicator for sun obscured. During periods of *B=1* when the cloud is present, a clear-sky index, k_c, is generated for each cloud present using distributions of clear-sky indices as a function of the okta number (Bright et al., 2015).

$$k_{ci} = f(okta) \quad \text{(eq. 9)}$$

The clear-sky index for overlapping clouds is found as the mean of the overlapping clear-sky indices

$$k_{ci}(\mathbf{B} = 1) = \frac{1}{c}\sum_{n=1}^{c} k_{c,n} \quad \text{(eq. 10)}$$

Where subscript *i* is the current iteration, k_c***(B=1)*** are the clear-sky indices during moments of cloud, $k_{c,n}$ is the k_c value for the n^{th} term, and c is the total number of overlapping clouds index.

The clear sky indices vector, $\boldsymbol{k_c}$, for each property is calculated at each iteration, *i*. This iteration, *i,* must undergo a correction as a function of *x'* and *u* to account for spatial variability, where *u* is the cloud speed; $\boldsymbol{k_c}$ is therefore calculated as

$$i = i + \frac{x'}{u} \quad \text{(eq. 11)}$$

$$\mathbf{k}_{ci}(B = 1) = kc_i \times \mathbf{F_1} \quad \text{(eq. 12)}$$

$$\mathbf{k}_{ci}(B = 0) = kc_i \times \mathbf{F_0} \quad \text{(eq.13)}$$

Multiple irradiance time-series can now be drawn from any *x-y-z* location within a 1.5 km by 3600*u* km area, each with different arbitrary plane orientations and tilts, such as the different tilts and rotations of residential PV installations within a low voltage grid. Irradiance is calculated for each location using the methodology outlined in Bright et al. (2015), and the corresponding clear-sky indices, $\boldsymbol{k_c}$, are applied.

2.4 Cloud Edge Enhancement

Cloud edge enhancement, CEE, describes events whereby a point on the surface receives a larger amount of incident irradiance than is available in the clear-sky irradiance, the events are attributed to irradiance reflecting from the edge of cloud. The typical behavior of irradiance in the 60 sec leading up to, and after the largest 1 sec ramps is detailed by Lave et al. (2012). This behavior is applied to periods of transitions from clear to clouded moments.

The CEE behavior is normalised to 1 to form a correctional factor for both ramp up, CEE_{up}, and ramp down, CEE_{down} as a function of a magnitude, *M*. The magnitudes of the CEE ramps are determined through analysis of 1-min data from the BSRN against the corresponding mean hourly weather observational data from the same location. The frequency and magnitude of ramp events attributed to CEE correlate with the okta number, CEE events were defined as >25% of the clear-sky irradiance. CDF profiles of the magnitude for each okta were made allowing for random extraction following the appropriate distribution. The normalised

CEE correction factors are further corrected as a function of *M*, which is itself a function of okta, as detailed in equations 14-16

$$M = f(okta, CDF) \quad \text{(eq. 14)}$$

$$CEE_{up} = CEE_{up} \times (1 + M) \quad \text{(eq. 15)}$$

$$CEE_{down} = CEE_{down} \times (1 - M) \quad \text{(eq.16)}$$

The application of the CEE is performed using the Boolean matrix of cloud presence, *B*. Iterating through k_c and using a logical if statement that queries whether *B* undergoes a ramp on account of cloud cover, the appropriate *M* adjusted CEE correction factor, CEE_{up} or CEE_{down}, are applied to the time before and after the ramp as shown in equations 17 and 18

$$B_{i=1} = 0 \;\&\; B_i = 1 \rightarrow k_c(i-60 : i+60) = CEE_{down} \quad \text{(eq. 17)}$$

$$B_{i=1} = 1 \;\&\; B_i = 0 \rightarrow k_c(i-60 : i+60) = CEE_{up} \quad \text{(eq. 18)}$$

3. Application and Discussion

To illustrate how the output could be used, the model is applied to a hypothetical configuration for the location of Cambourne, UK. Cambourne is selected as there is a BADC 1-min resolution irradiance data set (BADC, 2013) which will allow a temporal validation; figure 2 depicts the configuration.

Table 1 shows the physical parameter inputs required for each of the locations within the simulation. The x and y coordinates are noted in reference to the centre of the spatial domain, *C*,1 defined as (750,750). The azimuth angles are defined as -180° to 180° East to West, with South being an angle of 0°.

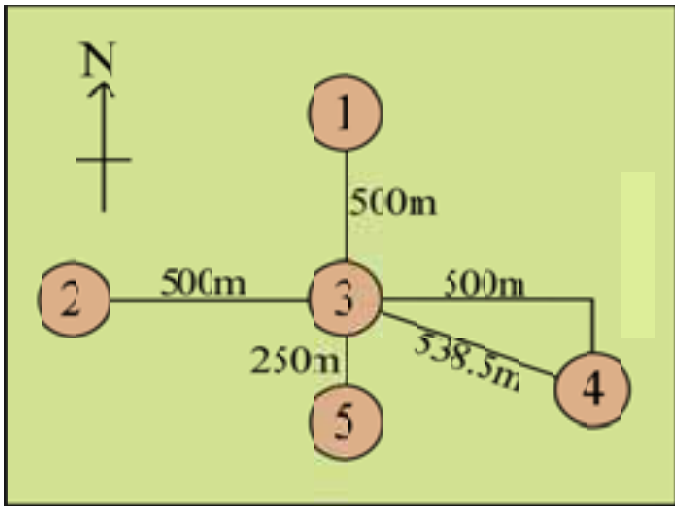

Fig. 2: A theoretical setup used to demonstrate the functionality of the model. The numbers indicate 5 different locations set in Cambourne, UK, of which spatio-temporally correlating irradiance time-series will be generated.

Tab. 1: Input physical parameters for the 5 locations as shown in figure 2. Note that the letter C denotes the centre of the spatial domain which represents *(750,750)*.

	1	2	3	4	5
x (m)	C	C - 500	C	C + 500	C
y (m)	C + 500	C	C	C - 200	C – 250
Azimuth *(°)*	0	0	0	0	0
Pitch *(°)*	0	0	0	0	0
Elevation *(m)*	87	87	87	87	87

The model is functional for all azimuth and tilts with reference to the input longitude and latitude, in this instance however the locations are assumed flat so that irradiance is reported in terms of global horizontal irradiance, the purpose of this is for comparison with the global horizontal observation irradiance data. The weather station in Cambourne, UK is at a longitude of -5.32656^{o} and latitude of 50.2178^{o}, with an elevation of 87 m above sea level.

The temporal resolution of 1 minute has a spatial granularity defined as the smallest distance between locations where a difference in irradiance can be observed. This is determined using the temporal resolution of *60 s* and the minimum and upper cloud speeds of *1* ms^{-1} and *~20* ms^{-1} to give a granularity of *60* to *~1200* m.min^{-1}. The average cloud speed is *10* ms^{-1} which gives typical granularity around *600* m.min^{-1}. The scenario depicted in figure 2 shows that the locations are separated by at least *250-1020* m and will therefore show appropriate differences. In order to observe spatially varying irradiance time-series for locations closer together, a decreased granularity would be required. This is achieved by increasing the temporal resolution e.g. from *60* s down towards *1* s.

Figure 3 displays a typical output from the model using inputs from table 1. The profile is typical of a clear day in mid-January for the location of Cambourne, UK. Typical patterns can be observed associated with the spatial correlation. Most notably around 700 minutes, there is a gradual ramp down in output at location 1 a few minutes before the other 4 locations undergo a similar ramp down, this is attributed to the wind speed and direction at the time, the clouds were travelling approximately north to south. At ~860 minutes, location 2 is the only location to undergo a large ramp down event.

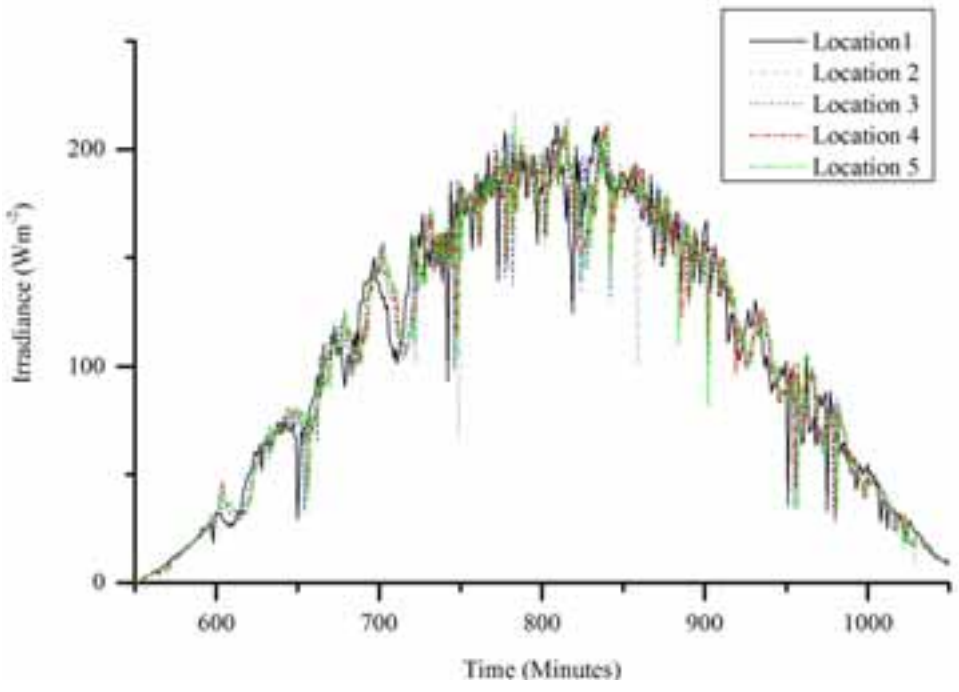

Fig. 3: Synthetic irradiance profiles across 5 locations on the 10th Jan using the described methodology for Cambourne, UK.

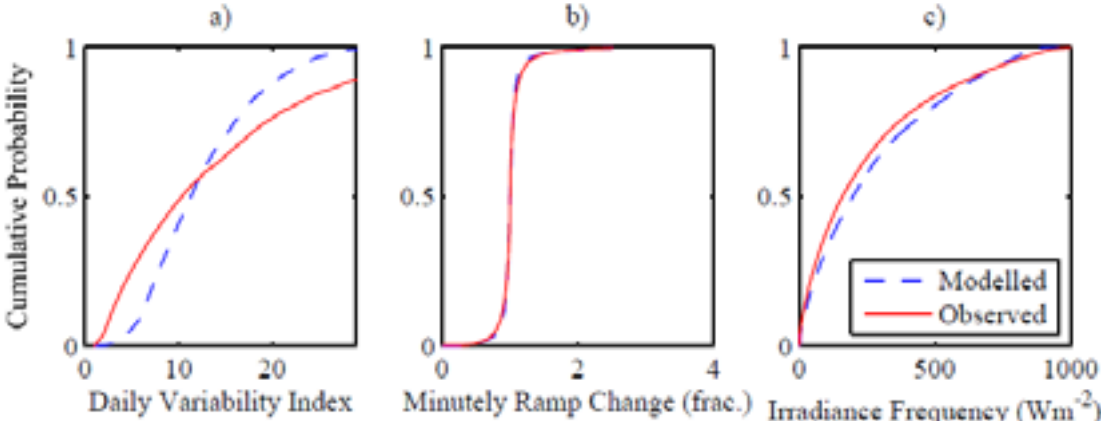

Fig. 4: Cumulative probability distribution plots of the (a) daily variability index, (b) the minutely irradiance ramp-up and ramp-down occurrences, and the (c) minutely global horizontal irradiance frequencies for both the modelled data and the measured data from Cambourne, UK.

4. Validation

Validation to date has focussed on a temporal basis only. All data processing was performed using the commercial software package Matlab r2012a (Matlab, 2012). Hourly weather observational data are taken from the BADC (BADC, 2013). As monitoring stations are occasionally taken off-line for repairs or upgrades for months at a time, 12 years of data are used to allow at least 10 years data for each variable that require a Markov chain to be created.

The simulation is run as detailed in the Application and Discussion section, and compared against the statistics obtained from the World Radiation Monitoring Centre – Baseline Surface Radiation Network (WRMC-BSRN, 2014) from BSRN station number 50, located in Cambourne, Cornwall, UK. Missing data points were ignored and deemed to not significantly impact the distributions for comparison.

Three metrics are used to validate the temporal nature of the model output, the variability index (Stein et al., 2012) cumulative probability function (CDF), the irradiance frequency CDF and the ramp rate CDF, denoted as VI, IF and RR respectively. The 2-sample Kolmogorov-Smirnov (K-S) test was carried out for each metric for each day of the year. When comparing the entire data sets against one another, the K-S validation technique is not appropriate due to the size. The subsets for comparison must be relatively small to gain any significant findings from the K-S test. For this reason the subset of each K-S test consisted of 7 of the same day's minutely data. For example, 7 modelled samples of the 1st January represent one subset, which is compared against a subset made from 7 samples of the same day from observational data.

The K-S test results are displayed in table 2 and comparative CDF profiles in figure 4. The RRs are captured well correlating with R^2=0.9998, and that 99.5% of days with the K-S test reject the null hypothesis that the modelled and observed minutely datasets are not from the same dataset with a confidence of 99%. The implications of this are that for each day of the year, only 0.5% of the days modelled did not produce statistically representative ramp rate data to a confidence of 99%. This means that for application of PV integration into the LV grid for example, the ramp rates seen in the synthetic irradiance time-series would be statistically accurate and allow for a good comprehensive study of how ramp rates impact upon the grid to a 1-min resolution. The daily VI CDF correlates with R^2=0.9777, and K-S at 95.9%. When comparing 1-min VI values for the whole datasets against one another in a frequency plot, the R^2 value is 0.9980 implying that throughout the year, the VI is captured, figure 4a however demonstrates that there is a more localised dependency with room for improvement. The daily VI value is the mean VI value recorded for that day. It can be seen that there is a slight overestimation of days with a VI between 7-15 and an underestimation of stable days between VI=0 to 7 and unstable days with VI >15, the implication of this is that the lower and higher daily variability extremes, where the variability is sustained over a lower time resolution, are slightly

Tab. 2: The percentage of days that reject the null hypothesis when performing the 2-sample Kolmogorov-Smirnov test on 7 of the same day of modelled and observational CDF profiles of 3 metrics.

K-S test significance Level	**90%**	**92.5%**	**95%**	**97.5%**	**99%**
Variability index	97.5%	97.5%	97.3%	96.4%	95.9%
Ramp rate occurrence	99.7%	99.7%	99.7%	99.7%	99.5%
Irradiance frequency	99.7%	99.7%	99.7%	99.7%	98.9%

less frequent than in reality. The VI is still captured at a satisfactory rate with K-S of 95.9% with only 4.1% of days accepting the null hypothesis that the observational and synthetic datasets are not the same, importantly of these 4.1% of days, there was no bias as to what time of the year these days occur, suggesting that there was no seasonal bias within the model. Potential reasoning is that within the observational data, a particular day for each of the 7 different years coincidentally had an overcast day each time, which when compared with a clear day generated by the model, would be dramatically unfavourably compared. The IF CDF correlates well with R^2=0.9980, and K-S at 98.9%. Figure 4c indicates a marginal overestimation in the lower range of irradiance magnitudes and a marginal underestimation in the extreme values of 900-1000 Wm^{-2}. The more extreme values within the models are functions of the clear-sky fluctuations and the cloud edge enhancements. It is possible that because the cloud edge enhancement correction described in section 2.4 only bands across 1-min before and after the CEE event, when in fact this 1-min is an average of all the events recorded within the study, it is entirely possible that a CEE event would span across 2 or more minutes depending on the speed of passing cloud, and so there is scope to make the correction a function of the cloud speed. Otherwise the validation is very strong and the magnitudes are captured well with only 1.1% of days accepting the null hypothesis with the K-S test.

5. Conclusion

This work has developed meaningful high temporal resolution irradiance time-series with a spatial correlation that temporally validates well. The irradiance time-series correlate spatially as a function of location, cloud speed and direction. The variability index, ramp rate occurrence and irradiance frequency metrics perform well using the 2-sample K-S test with a confidence level of 99%. The daily variability indices do tend towards midrange values, however the 1-minute variability index correlates excellently. The ramps present within the simulation have an excellent correlation to observation data with 99.5% of all days passing a 99% significance level K-S test.

Future work opportunities include further development of the temporal resolution as the nature of the methodology would allow it to be increased. This methodology would allow for theoretical high resolution simulations and studies of the impacts of solar variability and intermittency derived from readily available inputs of mean hourly weather observational data. The temporal methodology and Matlab script files are made freely available through download so that it can be adopted for any other application, and adapted to further the study (Bright et al., 2015).

6. Acknowledgments

This work was financially supported by the Engineering and Physical Sciences Research Council through the University of Leeds Centre for Doctoral Training in Low Carbon Technologies (Grant No.: EP/G036608/1).

7. References

BADC, 2013. British Atmospheric Data Centre – National Centre for Atmospheric Science – Natural Environmental Research Council. <http://badc.nerc.ac.uk> .

Bright, J. M., Smith, C. J., Taylor, P. G. and Crook, R., 2015. Stochastic generation of synthetic minutely irradiance time-series derived from mean hourly weather observation data. Sol. Energy **115**, 229–242.

Calinoiu, D-G., Stefu, N. Paulescu, M., Trif-Tordai, G., Mares, O., Paulescu, E., Boata, R., Pop N., and Pacurar A., 2014. Evaluation of errors made in solar irradiance estimation due to averaging the Angstrom turbidity coefficient. Atmos. Res. **150**, 69–78.

Ehnberg, J. and Bollen M., 2005. Simulation of global solar radiation based on cloud observations. Sol. Energy **78**, 157–162.

Gueymard, C. A., 2012. Clear-sky irradiance predictions for solar resource mapping and large-scale applications: Improved validation methodology and detailed performance analysis of 18 broadband radiative models. Sol. Energy **86**, 2145–2169.

Hummon, M., Ibanex, E., Brinkman G. and Lew D. 2012. Sub-hour solar data for power system modelling from static spatial variability analysis, Conference Proceedings in 2nd Annual Solar Integration Workshop, Lisbon. NREL/CP-6A20-56204.

Lave, M., Kleissl J., and Arias-Castro, E., 2012. High-frequency irradiance fluctuations and geographic smoothing. Sol. Energy **86**, 2190-2199.

Matlab 2012. Version 7.14.0.739 R2012a. The MathWorks Inc., Natick, Massachusetts.

Morf, H. 1998. The stochastic two-state solar irradiance model STSIM. Sol. Energy **62**, 101–112.

Morf, H. 2011. The stochastic two-state cloud cover model STSCCM. Sol. Energy **85**, 985–999.

Morf, H. 2013. A stochastic solar irradiance model adjusted on the Angstrom-Prescott regression. Sol. Energy **87**, 1–21.

Sayeef, S., Heslop, S., Carnforth, D., Moor, T., Percy, S., Ward, J. K., Berry, A., and Rowe, D. 2012. *Solar Intermittency: Australia's Clean Energy Challenge.* Tech. Rep., CSIRO.

Stein, J. S., Hansen C. W., and Reno, M. J., 2012. *The Variability Index: a new and novel metric for quantifying irradiance and PV output variability.* World Renewable Energy Forum, Denver, CO,.

Vindel, J. and Polo, J. 2014. Intermittency and variability of daily solar irradiation. Atmos. Res. **143**, 313–-327.

Widén, J., Carpman, N., Castellucci, V., Lingfors, D., Olauson, J., Remouit, F., Bergvist, M., Grabbe, M. and Waters, R. 2011. Variability assessment and forecasting of renewables: a review for solar, wind , wave and tidal resources. Renew. Sustain. Energy Rev. **44**, 356–375.

Wood, R. and Field. P. R.. 2011. The distribution of cloud horizontal sizes. J. Clim. 24. **24**, 4800–4816.

WRMC-BSRN, 2014, World Radiation Monitoring Center – Baseline Surface Radiation Network. PANGEA – Data Publisher for Earth and Environmental Science. <http://bsrn.awi.de/>.